IEEE Access
Multidisciplinary ⋮ Rapid Review ⋮ Open Access Journal

Received 19 December 2022, accepted 22 February 2023, date of publication 27 February 2023, date of current version 2 March 2023.

Digital Object Identifier 10.1109/ACCESS.2023.3249296

RESEARCH ARTICLE

Application of Artificial Neural Network-Based Tool for Short Circuit Currents Estimation in Power Systems With High Penetration of Power Electronics-Based Renewables

RAFAT ALJARRAH[1], MURAD AL-OMARY[2], DUA'A ALSHABI[2], QUSAY SALEM[1], SAHBAN ALNASER[3], DRAGAN ĆETENOVIĆ[4,5], (Member, IEEE), AND MAZAHER KARIMI[6], (Senior Member, IEEE)

[1]Electrical Engineering Department, Princess Sumaya University for Technology, Amman 11941, Jordan
[2]Energy Engineering Department, German Jordanian University, Amman 11180, Jordan
[3]Electrical Engineering Department, The University of Jordan, Amman 11942, Jordan
[4]Department of Electrical and Electronic Engineering, The University of Manchester, M13 9PL Manchester, U.K.
[5]Faculty of Technical Sciences Ćaćak, University of Kragujevac, 32000 Ćaćak, Serbia
[6]School of Technology and Innovations, University of Vaasa, 65200 Vaasa, Finland

Corresponding author: Mazaher Karimi (mazaher.karimi@uwasa.fi)

This work was supported by the University of Vaasa through the Centralized Intelligent and Resilient Protection Schemes for Future Grids Applying 5G (CIRP-5G) Research Project by Business Finland under Grant 6937/31/2021.

ABSTRACT The increasing integration of Power Electronics (PE)-based renewable energy sources into the electric power system has significantly affected the traditional levels and characteristics of fault currents compared to the ones observed in power systems dominated by synchronous generating units. The secure operation of a renewable rich power system requires the proper estimation of fault currents with wide range of scenarios of the high share of renewables. Although the utilization of detailed and complex time-domain dynamic simulations allows for calculating the fault currents, the resulting modeling complexity and computational burden might not be adequate from the operational perspective. Thus, it is necessary to develop alternative quicker data-driven fault current estimation approaches to support the system operator. For this purpose, this paper utilizes an Artificial Neural Network (ANN)-based tool to estimate the characteristics of short circuit currents in power systems with high penetration of power electronics-based renewables. The short circuits against different penetration of renewables are produced offline using the DIgSILENT PowerFactory considering the control requirements for renewables (e.g., fault ride through requirement). The resulting dataset is utilized to train the ANN to provide the mapping between the penetration level and the characteristics of the short circuit currents. The application of the approach using the modified IEEE 9-bus test system demonstrates its effectiveness to estimate the components of short circuit currents (sub-transient current, transient current, and peak current) with high accuracy based only on the penetration of power electronics-based renewables.

INDEX TERMS Artificial neural networks, future power systems, photovoltaic systems, power electronics, short circuit currents.

I. INTRODUCTION

These days usage of renewable energy sources (RESs) has grown rapidly over the years and become an important part of the electrical industry. The increased penetration of RESs, e.g., wind and PV, has the potential to change the traditional dynamics and properties of the power system from those which have been usually observed in synchronous generators (SGs)-based conventional power systems [1], [2], [3]. Short circuit (SC) currents are considered one of the system's

The associate editor coordinating the review of this manuscript and approving it for publication was Mu-Yen Chen.

characteristics that have the potential to be altered due to the different fault contributions from the RESs in comparison with the conventional SGs [4]. This is caused by the Power Electronic (PE) converters that are used for grid integration. Such PE converters are subjected to the limitation in terms of their fault current-currying capability to avoid stressing the switches, e.g., IGBTs [5]. Hence, their SC currents contribution would be remarkably different from the one fed by SGs [6], [7], [8], [9]. In return, this will result in different levels and characteristics of SC currents in renewable-rich power systems. As for PE-based RESs, their fault currents contributions have been usually neglected assuming an imperceptible effect on the accuracy of the calculations. However, this might not be applied to renewable-rich power systems. This is also driven by the grid codes which have recently started to define the Fault-Ride-Though (FRT) requirement. FRT requires that RESs must remain connected during fault events and provide dynamic voltage support by injecting reactive currents during faults [10], [11], [12], [13]. Hence, the SC contribution from RESs shows distinct characteristics due to the limitation in their current-carrying capability, the different control strategies, and the various FRT requirements.

A lot of research work has been done and reported regarding the topic of SC current contribution from RESs. While some of the reported work has delivered a good perception of the differences between the SC contribution of RESs and the conventional SGs [14], other studies have tackled the issue of modeling of RESs during fault calculations [15], [16], [17]. Moreover, a decent number of studies have suggested methods for the calculation of the fault currents in power systems considering the contribution from the RESs [18], [19], [20]. Although reported studies have provided good insight into the characteristics of SC currents of RESs and their impact on the fault level in high RESs-rich power systems, there is still a need to better correlate the SC currents with the penetration level to achieve more understanding and accurate estimation of the SC current components, trends, and behavior in the future power systems.

On the other hand, in recent literature, research on understanding the behavior of SC currents during faulty events in power systems with a high share of RESs is emerging. For instance, new mathematical-based analysis for fault level calculation under high penetration of RESs have been proposed in [19]. In [21], the study has also investigated the sensitivity of the SC currents characteristics to the penetration level of RESs. It was suggested that the dynamic characteristics of the SC currents are significantly affected and altered according to the penetration level of RESs.

This has called for more research on estimating the SC characteristics in renewable-rich power systems. Traditional fault level calculation methods utilize steady-state modeling which has been providing decent approximate results for conventional SGs-based power systems. Such methods have been built based on the physical performance of the SGs during faulty conditions where SGs are modelled as voltage sources behind impedances. To an extent, such modeling has been capable of estimating the dynamic characteristics of the time-decaying SC currents fed by conventional SGs.

The new version of the IEC 60909 standards [22], which are commonly used in a major part of the world due to their simplicity, provides guidance on how to account for such contributions, especially in the case of high integration of RESs. For example, RESs that utilize Full-Size Converters (FSCs), such as PV systems, have been modelled as current sources with a fixed fault contribution bounded by the maximum overrating capability of the converter [23]. A modified IEC-based method for considering the fault contribution of RESs has been also proposed in [24], where the FSCs-based RESs have been modelled as a current source considering the dynamic voltage support and the injected reactive current more accurately.

It is worth noting that all the previously mentioned research and standards require detailed modeling or time-consuming time-domain simulations in order to observe the potential changes in the characteristics of the SC currents in future scenarios. Moreover, and according to the authors' best knowledge, there is no artificial intelligence-based application proposed to estimate the characteristics of the SC currents based on the penetration level of RESs. Hence, this research proposes an Artificial Neural Network (ANN)-based tool that can estimate the altered dynamic characteristics of the SC currents in renewable-rich future power systems without a need for such detailed modeling or repetitive fault calculations. Using an AI-based tool, more specifically ANN, for SC currents estimation is motivated by the proven efficacy of using ANNs when applied in power system problems for input-output mapping such as pattern recognition, forecasting/estimation, classification, and function approximation [25], [26], [27]. For example, researchers in [25] have used an ANN-based tool for forecasting power system inertia in a high share of wind energy. Their results have shown the capability of the developed ANN-based tool to forecast the system inertia with various penetration scenarios accurately. Other research in [27], has demonstrated the superiority of the ANN among the other AI techniques when applied for short-term forecasting. Moreover, ANNs have advantageous characteristics among other AI methods in terms of the ability to adapt and learn by example in real-time, fast speed, and generalization.

In this paper, the proposed algorithm directly correlates the penetration level of RESs with the SC characteristics by utilizing the power system topology as well as the variables measured by phasor measurement units. It provides a fast, simple, and straightforward tool for tracking the altered dynamic characteristics of the SC currents in renewable-rich power systems.

Such a tool would also enable researchers and system operators to achieve a better understanding of the future changes/alterations that might be observed in the SC characteristics by using the penetration level as the only input

variable in their network. Such a proposed ANN-based tool would also benefit planning engineers and system operators by providing a fast and straightforward scanning tool that allows determining the SC level that might be available when scheduling (bringing online/offline) the generation units. Hence, avoiding weak grid points and marinating the required minimum SC level to keep stable operation conditions.

The rest of the paper is structured as follows: Section II, introduces the SC currents calculation and the Power Electronics-based RESs modeling according to the IEC 60909 standards. Section III introduces the concept of development and application of ANN for SC current estimation. Section IV presents the proposed ANN-based algorithm for SC's current estimating tool. Section V discusses the simulation results and validates the accuracy of the proposed algorithm, and finally, Section VI concludes the paper.

II. OVERVIEW OF SC CURRENTS CALCULATION BASED ON THE IEC 60909 STANDARDS

The fault calculation based on the latest version of the IEC 60909 standards uses the Thevenin equivalent to calculate the SC current without considering the RESs. Next, it uses superposition for calculating the SC current contribution of the PE-based RESs, which are modelled as current sources. Fig. 1 shows the characteristics of the SC currents under study including the maximum initial symmetrical SC current I_k'', the peak instantaneous current I_p, and the breaking current I_b, which are obtained for each considered scenario of RESs penetration.

A. CALCULATING THE FAULT CURRENT FROM SGs ONLY

At first, the IEC 60909 standards have been used to calculate the initial symmetrical SC current I_k'', without considering the fault current contribution from the RESs in the system. This calculation is based on the Thevenin equivalent utilizing the network topology and the network reduction. The initial symmetrical fault current I_k'' is calculated using the Thevenin

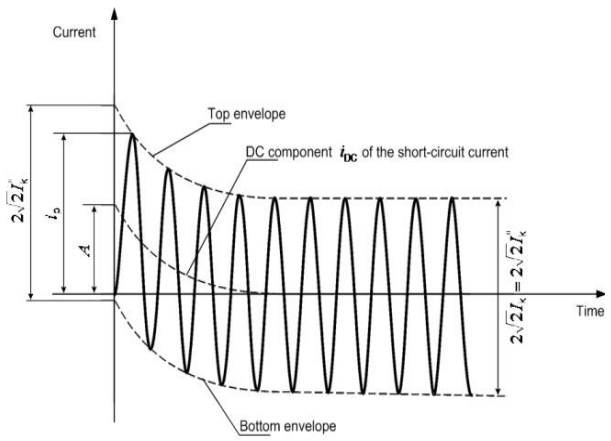

FIGURE 1. Short Circuit Current Components according to IEC 60909 Standards [22].

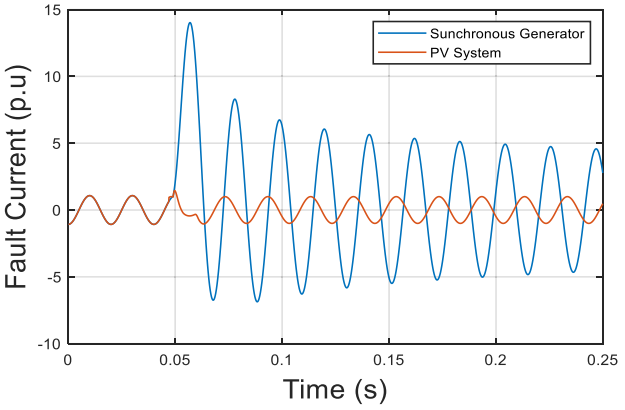

FIGURE 2. A typical waveform of short circuit currents a PV generator and a synchronous generator with the same ratings.

equivalent impedance at the faulty point Z_k in addition to the pre-fault voltage according to equation (1), where c is a voltage factor that is used to scale the equivalent voltage source in the calculations to account for variations in the system voltage, V_N and V_L are the phase and the line voltages, respectively.

$$I_{k''} = \frac{c \times V_N}{Z_k} = \frac{c \times V_L}{\sqrt{3} \times Z_k} \tag{1}$$

B. MODELING AND CALCULATING THE FAULT CURRENT FROM PE-BASED RESs

As mentioned above, the fault current contribution of PE-based RESs, such as PV systems, is limited and may show a very fast transient followed by a fixed component. Such characteristics are significantly different from those observed from traditional SGs as shown in Fig. 2. According to the latest version of IEC 60909 standards, the fault current contribution of the PE-based RESs, represented by the PV systems, IPV_{SC}, is calculated by modeling this source in the positive-sequence system as a current source with infinite impedance. The value of the current depends on the type of short circuit and must be provided by the manufacturer. However, it is typical to assume that the maximum current injected by the PV, IPV_{max}, is bounded between 1-1.4 p.u. of the rated current of the PV system [2]. This is to mimic the fault current contribution that is limited in order to protect the switches of the inverter interface utilized for the grid connection. Note that the positive-sequence infinite impedance Z_{PV} is assumed to be shunt connected; hence, it is neglected, and it does not affect the fault contribution from the PV generator to the faulty bus. The exact fault current contribution to the faulty point depends on both the transfer impedance between the PV source and the faulty point as well as the Thevenin equivalent impedance of the faulty point itself, as given by (2).

$$IPV_{SC} = \frac{1}{Z_k} \sum_{j=1}^{j=M} Z_{ij} \times IPV_{max} \tag{2}$$

where:

- M is number of the connected PV systems,
- $IPV_{\max}$ is the maximum fault current contribution of the PV system connected to the j^{th} bus,
- IPV_{SC} is the total fault current contribution of all connected PV systems,
- Z_{ij} is the transfer impedance between the bus j and the faulty bus i,
- Z_k is the equivalent impedance at the faulty bus k.

III. THE PROPOSED ALGORITHM OF THE SC CURRENT ESTIMATING TOOL

The proposed algorithm for estimating the characteristics of the SC currents in PE-rich power systems depend basically on collecting a large data of the different components of the SC current in a large number of scenarios of PE-based RESs penetration. The dataset that has been used for feeding the inputs of the developed ANN are collected from simulating many scenarios of PE-based RESs penetration level into the network under study. These scenarios have covered a wide range of PE-based RESs (i.e., PV systems) penetration p starting from $p = 0\%$, where the whole installed generators are conventional SG-based, up to a maximum penetration level of $p = 100\%$, where all SGs are replaced by PV generators. During this data collection stage, the studied system would be first modelled in DIgSILENT PowerFactory software and then analyzed using Matlab. The dataset covers the selected components of the SC currents that are calculated based on the IEC 60909 standards described earlier (Section II), in addition to the online-measured penetration level of PE-based RESs. It is worth mentioning that the RESs utilized here are composed of generic models of PV systems available in DIgSILENT PowerFactory. They are modelled as a current source with a maximum fault current contribution of 1.2 p.u. of their rated currents to account for their fault contribution according to the IEC 60909 standards. The penetration level (p) is defined based on the rating capacity of the installed PE-based RESs as a percentage of the completely installed generation capacity of the system according to (3).

$$PV\ Penetration = p = \frac{PV_s}{PV_s + SG_s} \times 100\% \qquad (3)$$

where, SGs and PVs represent the installed capacity of the SGs and PV systems, respectively. Next, these collected data will be fed to the developed ANN to be trained in order to provide the required mapping between the penetration level and the studied characteristics of the SC currents. After achieving the target accuracy by measuring the Mean Square Error (MSE) of the trained ANN, the developed ANN will be tested and validated for randomly chosen values of the penetration level (p). The overall algorithm for the SC current estimation tool comprises five steps. The first step is modeling the test system in DIgSILENT PowerFactory software where SC current calculations are conducted according to the IEC 60909 standards. The second step is generating the suggested scenarios which include the different penetrations of PV systems and decommissioning of the SGs.

The third step is conducting SC current calculations on the selected scenarios using the IEC 60909 standards in order to collect the required large dataset of SC current components considering the SC contribution of SGs and PV systems. Forth step is the development and construction of an appropriate ANN for SC current estimation. At the fifth step, where careful consideration has been taken for the ANN architecture, the proposed ANN is trained to map between the input (represented by penetration level percentage p) and the output (represented by the generated dataset of SC current components) using the various scenarios under the study. Finally, validation and testing of the trained ANN are conducted using randomly selected inputs that represent new scenarios between 0% and 100% penetration levels other than those scenarios used for the ANN training stage. These testing scenarios are described in more detail in the results section. The flowchart of the proposed algorithm is shown in Fig. 3.

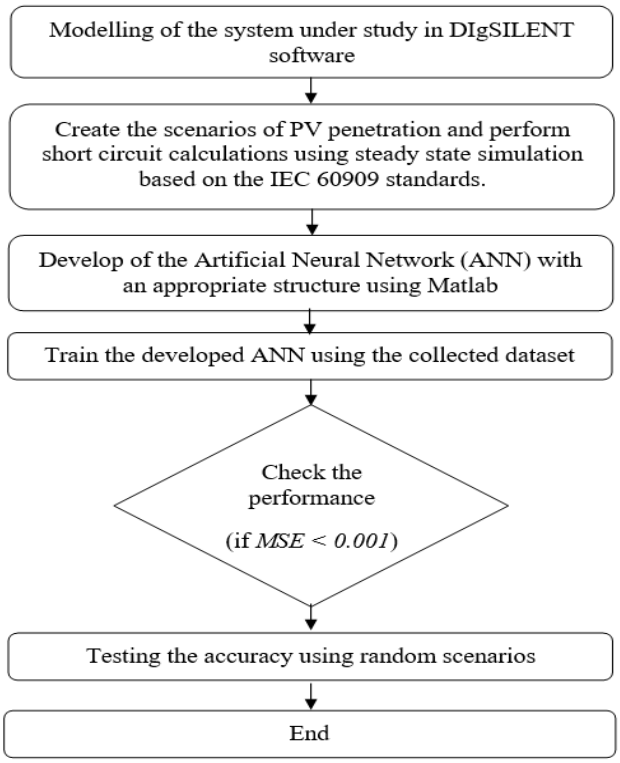

FIGURE 3. A Flow chart of the proposed ANN-based SC estimation tool.

IV. DEVELOPMENT OF THE ARTIFICIAL NEURAL NETWORK

ANN is a well-known data processing system that consists of highly interconnected elementary units, called neurons, which are connected in a number of layers and work in parallel. The most critical part of the implementation of a neural network is the selection of the structure, which is also referred to as its architecture, as it affects the accuracy of

the results which are going to be obtained from the trained network. The basic structure is the one in which units are distributed in three-layer types: an input layer, an output layer, and one or more hidden layers [28].

In this work, a multilayer feed-forward back propagation (FFBP) ANN has been developed for estimating the characteristics of the SC currents in the system under study. FFBP networks are commonly used and suggested in the literature for input-output mapping problems such as pattern recognition, classification, and function approximation [25], [26]. ANNs consist of a series of layers in a form of input, hidden, and output layers. While the first layer has a connection from the network input, each subsequent layer of the hidden layers has a connection from the previous layer. The final layer in its turn produces the network's output. Such ANN can be used for any kind of input to output mapping. Each of the hidden and output layers includes sets of neurons that are connected to the neurons in the subsequent layer. The number of hidden layers as well as the neurons is problem-dependent that are mostly determined by trial and error till a goal performance is achieved [29]. However, this should be selected based on the careful consideration to achieve a stable ANN. For instance, an excessive number of hidden neurons may cause overfitting meaning that the ANN has overestimated the complexity of the target problem [30]. A competent network architecture might be determined depending on the dimensions, features and complexity of the problem. In some cases, a smaller number of layers/neurons would be enough to achieve the minimum target error. For example, an ANN with one hidden layer and enough neurons can fit any finite input-output mapping problem. Fig. 4 shows the typical architecture of a neuron and a multi-layered ANN.

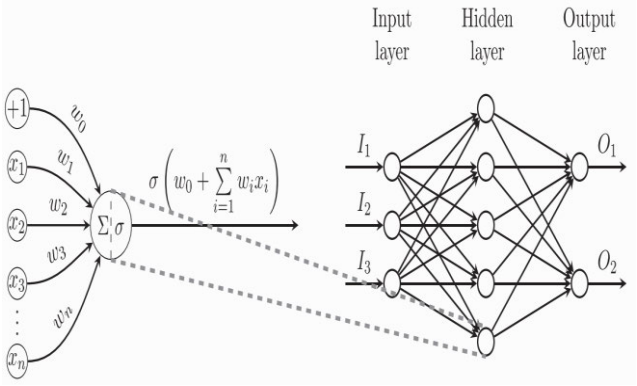

FIGURE 4. The typical structure of an artificial neural network [25].

The input layer of the ANN is fed by the inputs, which are directly sent to the neurons in the hidden layer after being modified by some weight coefficients. This process will be repeated as the neurons of the first hidden layer pass their weighed output to the neurons of the subsequent layer until reaching the output layer in the designed ANN. In this work, the inputs are represented by the values of the penetration (p) reflecting the PV penetration scenarios, where the outputs are represented by the SC current components extracted from the calculated SC current at different nodes in the system considering various scenarios. Six outputs (3 at each bus) are represented by the sub-transient SC current, I''_k, the transient SC current, I'_k, and the peak SC current, I_p, corresponding to each scenario.

V. RESULTS AND DISCUSSION

A. MODELING THE MODIFIED IEEE 9-BUS TEST SYSTEM IN DIgSILENT POWERFACTORY

The IEEE 9-bus test system [31] is modelled in DIgSILENT PowerFactory to perform the SC currents calculations for collecting the data required for the developed ANN. The system consists of 9 buses, six lines, three generators, three transformers, and three loads. The nominal voltage of the transmission buses is 230 kV, and the nominal frequency is 60 Hz. The SC calculations have been done by simulating the system under different scenarios of PV penetration. Initially, the system is fed by SGs only. Then, the RESs (i.e., PV systems) have been introduced in a step of 5% penetration to displace the SGs at all generation locations. Hence, 200 PV penetration scenarios have been simulated accordingly. The three components of the SC currents under study have been obtained at two selected buses in the system, namely bus 5 and bus 8 using the modified IEC 60909 standards explained above. Note a three-phase bolted fault has been assumed in all scenarios in order to obtain the maximum fault currents. Fig. 5, shows the adjusted IEEE 9-bus test system with the installed PV systems at the generation buses.

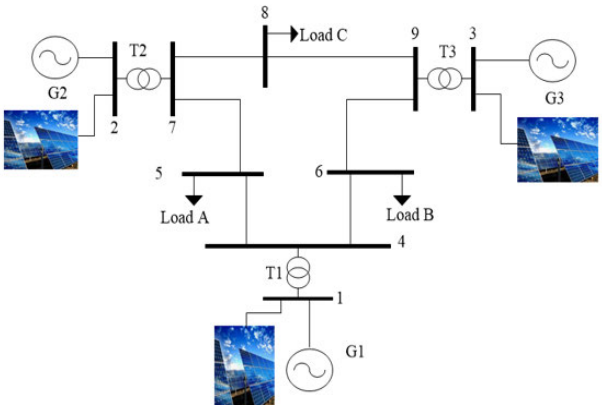

FIGURE 5. The Modified IEEE 9-bus test system.

B. GENERATING THE RESULTS OF THE SC CURRENTS AT DIFFERENT PV PENETRATION SCENARIOS

The modified IEEE 9-bus test system has been utilized to perform the SC currents calculations for collecting the data required for the developed ANN. The simulated scenarios have considered the installation of PV systems at all generation buses with the decommissioning of the existing SGs in such a way to keep the total generation capacity fixed. Note that the PV systems are assumed to be operating at power

factors like those of displaced SGs, hence supplying both active and reactive power. The amount of the supplied power of these PV systems is picked in such a way as to equal the amount of the power of the decommissioned SGs. The generated scenarios include calculating the corresponding fault current contribution of each SG, each PV system, and the total fault current at the selected buses. For illustration purposes, Bus 5 and Bus 8 are adopted to represent the variations in fault levels as shown in Fig. 6 and Fig. 7, respectively.

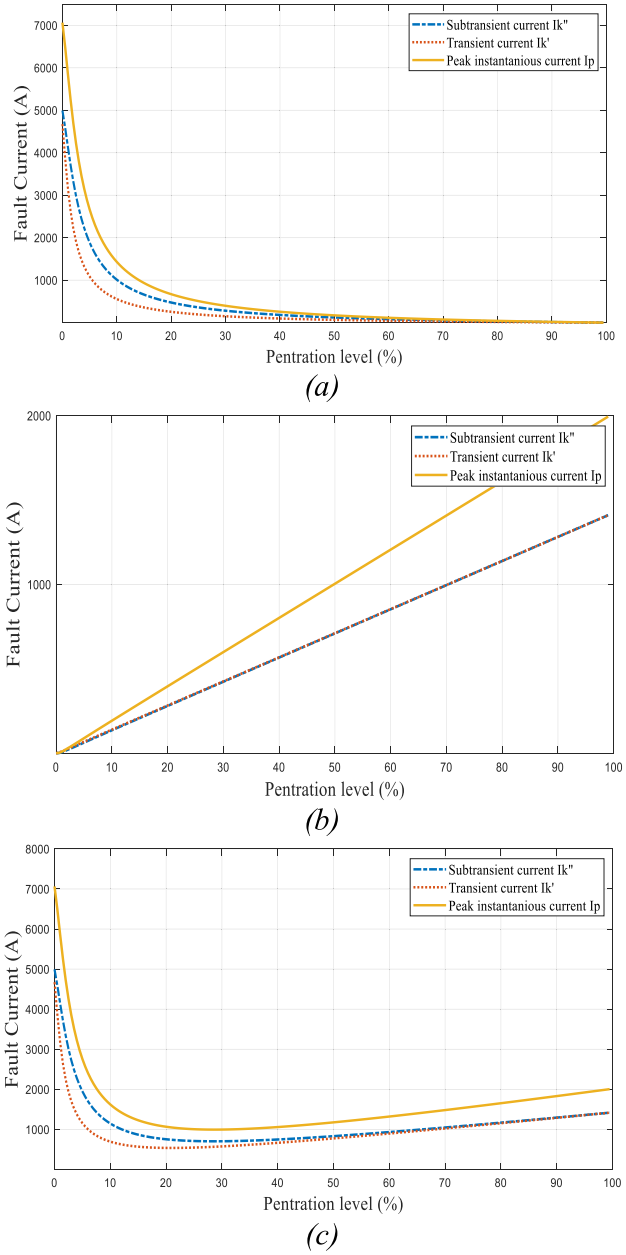

FIGURE 6. The SC currents at Bus 5 with different penetration percentages (a) fed from SGs, (b) fed from PVs, (c) fed from SGs and PVs.

This cover extracting three components of the SC current, namely, the sub-transient SC current, I_k'', the transient SC current, I_k', and the peak SC current, Ip, corresponding to each

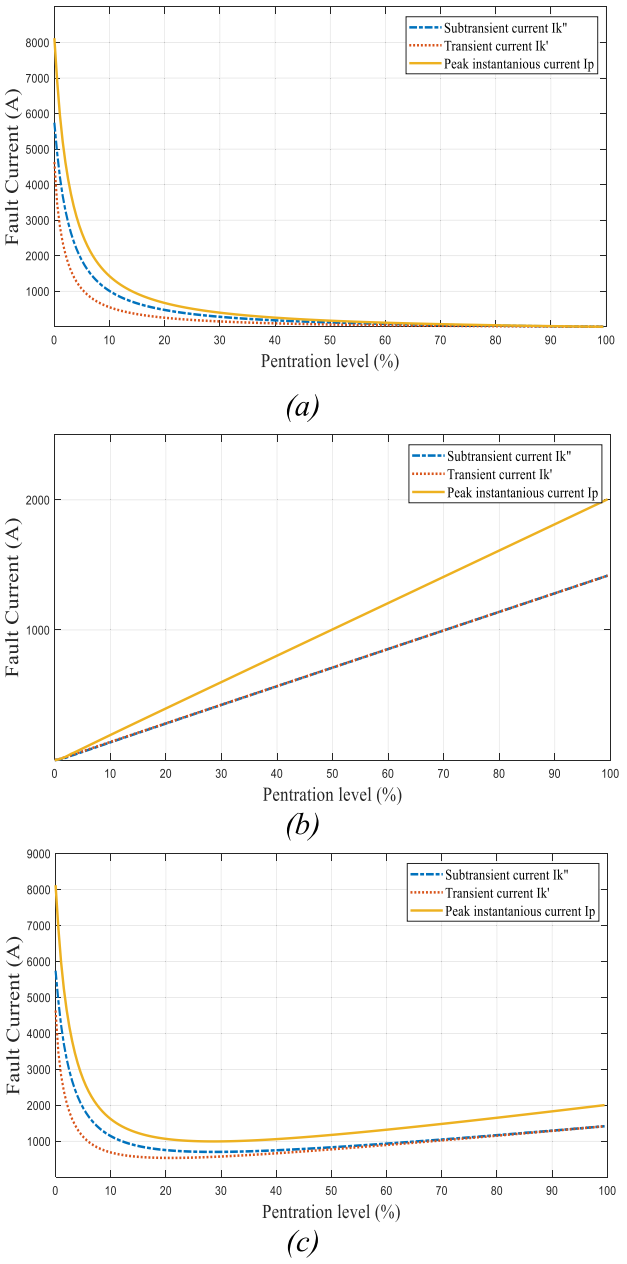

FIGURE 7. The SC currents at Bus 8 with different penetration percentages (a) fed from SGs, (b) fed from PVs, (c) fed from SGs and PVs.

scenario. It can be observed that all components of the SC current fed by SGs have witnessed a decline with the increased penetration level of PVs on both studied Buses, as shown in Fig.6.a, and Fig.7.a. On the other hand, the components of the SC currents fed from PVs have increased with the increased penetration level of PVs, as shown in Fig.6.b, and Fig.7.b. While the components of the SC current contribution of SGs decrease exponentially, it can be noticed that the components of the SC current contribution of PVs increase in a linear relationship with the increased penetration scenario. This confirms the different characteristics, hence the different modeling of these two different types of generation in terms

of the SC contribution. As the value of the decommissioned SGs might be reflected as an increase in the generator equivalent impedance with fixed rating, the value of the current source model of the PVs is proportionally increasing with the increased penetration scenario accordingly.

C. STRUCTURE OF THE PROPOSED ANN

The proposed ANN in this work is basically structured of three layers using Matlab software as shown in Fig.8. The input layer is the receiver of the input values, which is represented by the penetration level of RESs "p" in our work. Note that the nodes of the input layer are passive, meaning that they duplicate each value and then send it to the hidden nodes without performing any numerical processing. These nodes are fully connected to the hidden layer nodes using synaptic weights links that would be later adjusted through a learning procedure to improve the network performance. Similar weighted links exist between the hidden and the active nodes of the output layer, where they combine and change the data to produce two sets of three outputs as follows: the sub-transient SC current, I_k'', the transient SC current, I_k', and the peak SC current, Ip, for each of the studied bus 5 and three for the bus 8. It is worth mentioning that the number of neurons and hidden layers is problem-dependent and can be determined by trial and error till a goal performance (e.g., MSE) is achieved. In this research, one hidden layer is chosen while the number of neurons is nominated after careful testing in such a way as to achieve the minimum training error. Fig. 9, shows the developed ANN in Matlab. During the structuring process, where one hidden layer of feed-forward network with "logsigmoid" activation function and linear output neurons (fitnet) is chosen, several MATLAB simulations are run to find the proper number of hidden neurons in the hidden layer that would provide a proper fit this multi-dimensional mapping problem properly. Hence,

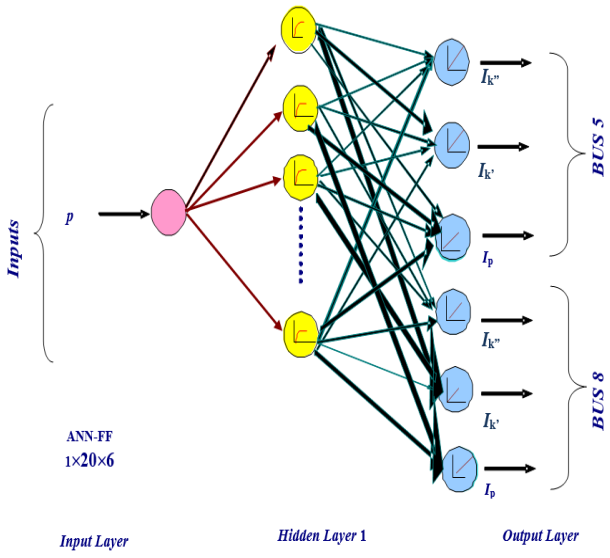

FIGURE 8. The proposed topology of the ANN.

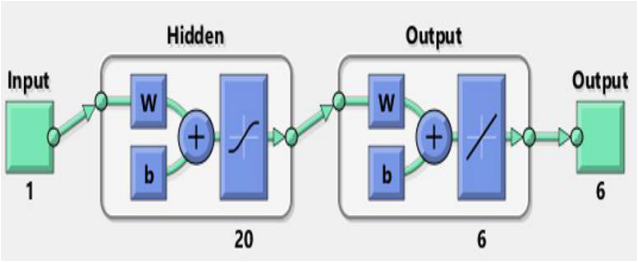

FIGURE 9. The calculated SC currents at Bus 8 with different.

different numbers of neurons (e.g. 10, 20, 25, and 30) have been tested in this work.

D. TRAINING AND VALIDATION OF THE PROPOSED ANN

Initially, the weights of the neurons of the adopted ANN are initialized with small random numbers when the network is first created. After that, the output dataset of the SC current components has been normalized to their initial maximum values at the base scenario before being fed to the network for determining the newly updated weights in what is called the training or learning process. As supervised learning is employed in this developed ANN, it is required to teach the unlearned network for input/output mapping, hence sets of input/output patterns are linked by adjusting weights using an appropriate training algorithm. It is worth noting that the size of the learning dataset has to be suitable to the complexity of the model to avoid overfitting which may occur during the training stage. In this work, 200 samples of output associated with each of the current components described above, which represents 200 scenarios of PV penetration, are chosen for training, validation, and testing of the results obtained at each bus. The collected dataset is divided into 70% training, 15% validation, and 15% testing, respectively. Hence, 70% of samples are fed to the network during training, where the network is adjusted in such a way as to minimize the cost function. The goal is to achieve the best training performance by minimizing a prescribed error measure (i.e., the cost function), which is reflecting the difference between the target and the predicted outputs of the network as possible. Note that the statistical indicator, MSE, is used as a cost function during the learning process to determine the best training performance, which tries to minimize the average squared error between the network's output and the desired output. Bedside that, the best structure (i.e., the number of neurons) has been identified based on the best combination of both the values of the MSE and the Regression (R). It is worth mentioning that the optimal value of this indicator is targeted to (MSE=0, and $R = 1$). Note that ($R = 1$) means a linear relationship between the input and the output, hence an optimal fitting, while (R=0) represents a random relationship and a poor fitting. Hence, the closer MSE to zero, and R to zero, the better the structure and the training accuracy. The results show that the minimum training error has been noticed when a hidden layer of 20 neurons is used where it has been found the most suitable as shown in Table 1.

The 15% of the validation samples are used to measure network generalization, and to halt training when generalization stops improving. On the other hand, the testing phase where 15% of the samples have been used independently, can provide an independent measure of the ANN performance during and after training without any effect from the training phase. It is worth pointing to the effect of the training algorithm on the accuracy and speed of the training process. In this regard, the effects of the training algorithms such as Bayesian Regularization (trainbr) and Levenberg-Marquardt (trainlm) have also been investigated in this work. While the first algorithm (i.e., trainbr) typically requires more time, it may lead to better generalization for difficult, small or noisy datasets. Note that the training through trainbr stops according to adaptive weight minimization.

On the other hand, trainlm algorithm requires more memory but less time as its training would automatically stop when the generalization stops improving, as indicated by an increase in the MSE of the validation samples. The detailed evaluation results of the training, validation, and testing phases of the simulated ANN are presented in Table 1. It can be seen that an ANN with 20 neurons in the hidden layer provides the best performance in terms of the MSE and R when trained using the trainbr training algorithm where the minimum gradient was reached at all iterations as highlighted in gray in Table 1. Observe Fig.10 which also shows the value of R of 0.99999 and the function fit of element 1 (i.e., I_k'' at bus 5).

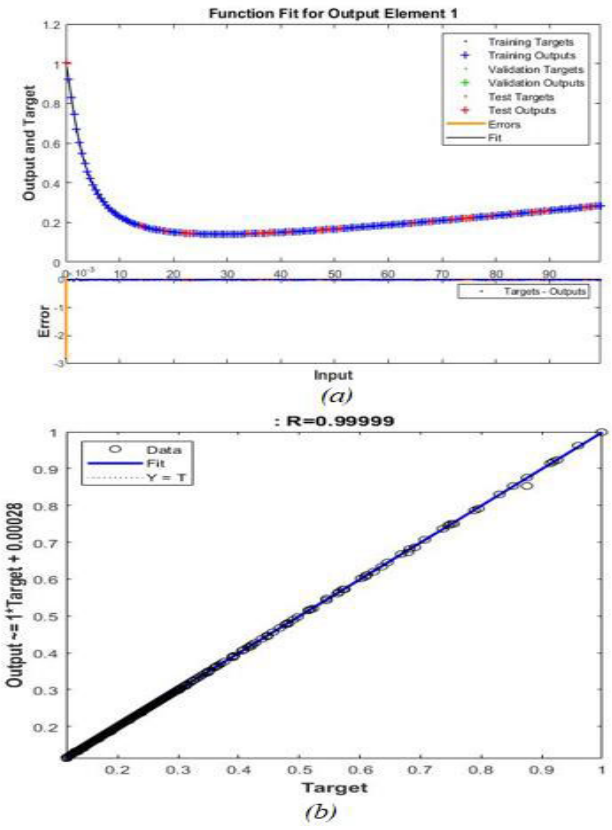

FIGURE 10. The ANN performance (a) the regression R values function fit.

E. TESTING OF THE PROPOSED SC CURRENT ESTIMATION TOOL USING RANDOMLY CHOSEN SCENARIOS

Evaluating the constructed model is an essential step used once the model is completely trained. Hence, the generalization capability of the proposed ANN-based SC current estimation tool is examined using new input/output testing pattern sets of different percentages of PV penetrations obtained from untrained scenarios. This step provides an independent measure and an extra testing for the performance of that developed tool. Each new scenario is simulated, and the actual values of the SC current components have been extracted at each of the studied buses. These scenarios are then fed to the developed ANN to obtain the estimated/predicted values correspondingly. Note that 30 random samples of the penetration level, p, have been fed to the input of the network, and 2 sets of (3 SC current components at each bus) are predicted are obtained as outputs. The results obtained from the simulations and those obtained from the ANN-based estimation tool have been tabulated in Table 2 and 3 for the analysis and performance comparison at buses 5 and 8, respectively. While the absolute error between the actual and predicted values of each component of the SC current is calculated in each scenario, the mean absolute percentage error (MAPE) is calculated for all the estimated values together as expressed in (4).

$$MAPE = \frac{1}{N}\sum_{p=1}^{N}\frac{SC_p^{Actual} - SC_p^{Predicted}}{SC_p^{Actual}} \times 100 \quad (4)$$

where, SC_p^{Actual}, is the actual SC current component obtained from the simulation. $SC_p^{predicted}$, is the predicted SC current component obtained from the ANN-based estimation tool. N, is the number of penetration scenarios. Observe Table 2 which presents the comparison results of the actual and the estimated values of the SC current components at Bus 5. Note that a set of 30 scenarios represented by the different values of the penetration percentage p, is tested. These have been randomly chosen in such way to cover the whole range of the penetrations between 0 and 100%. Note that the values in the Table of all the current components are normalized to their corresponding maximum values initially at the base scenario ($p = 0\%$). Hence, to calculate the values of these current components at Bus 5, in Amber (A), they have to be multiplied by the original maximum values as follows: $I_k'' = 4994.65$ A, $I_k' = 4675.18$ A, and $Ip = 7063.502$ A. It can be observed that the ANN-based estimation tool has provided predicted values with marginal errors in comparison with the actual values obtained from the simulations according to the IEC 60909 standards. Observe the maximum absolute error corresponding to each of the SC current components, as marked in bold in Table 2. While a maximum error of 0.0428 has been registered for the component I_k'', higher absolute errors of 0.055 and 0.058 have

TABLE 1. Performance indicators of the trained ANN.

No.	Hidden Layer Neurons	Training Performance		Testing Performance		Training Function	Number of epochs	MU	Gradient
		MSE	R	MSE	R				
1	10	3.3e-7	9.999e-1	5.12e-5	9.990e-1	trainlm	118	0.001	0.682
2	10	2.4e-10	9.998e-1	4.00e-10	9.999e-1	trainbr	470	0.005	0.654
3	20	1.32e-6	9.999e-1	2.078e-6	9.998e-1	trainlm	31	0.001	0.852
4	20	5.30e-11	9.999e-1	2.34e-12	9.999e-1	trainbr	432	0.005	1.45
5	25	2.05e-7	9.998e-1	7.12e-7	9.994e-1	trainlm	36	0.001	1.11
6	25	9.09e-11	9.999e-1	4.90e-6	9.999e-1	trainbr	235	0.005	2.34
7	30	4.91e-7	9.998e-1	4.54e-7	9.996e-1	trainlm	30	0.001	1.52
8	30	3.33e-11	9.999e-1	3.58e-10	9.999e-1	trainbr	459	0.005	1.42

TABLE 2. Validation of the Proposed ANN-based SC Estimation Tool at Bus 5.

No.	*p*	$I_{k"}$			I_k			Ip		
		SC_p^{Actual}	$SC_p^{Predicted}$	*Error*	SC_p^{Actual}	$SC_p^{Predicted}$	*Error*	SC_p^{Actual}	$SC_p^{Predicted}$	*Error*
1	0.75	0.875	0.875	0.0000	0.755	0.756	0.000	0.875	0.875	0.000
2	3.25	0.521	0.522	0.0010	0.345	0.345	0.000	0.521	0.522	0.000
3	5.25	0.375	0.377	0.0021	0.237	0.238	0.002	0.375	0.377	0.002
5	11.25	0.197	0.211	0.0137	0.133	0.139	0.005	0.205	0.211	0.005
6	12.25	0.192	0.198	0.0063	0.106	0.133	0.026	0.172	0.198	0.026
7	14.75	0.144	0.176	0.0315	0.116	0.123	0.007	0.169	0.176	0.007
8	19.25	0.133	0.153	0.0206	0.110	0.116	0.006	0.147	0.153	0.006
9	24.25	0.115	0.143	0.0284	0.106	0.116	0.011	0.132	0.143	0.011
10	28.75	0.111	0.141	0.0295	0.107	0.121	0.015	0.126	0.141	0.015
11	34.75	0.122	0.144	0.0217	0.104	0.132	0.027	0.116	0.144	0.027
12	39.75	0.135	0.150	0.0146	0.136	0.142	0.006	0.143	0.150	0.006
13	43.25	0.143	0.155	0.0117	0.133	0.150	0.016	0.138	0.155	0.016
14	47.25	0.105	0.161	0.0563	0.153	0.159	0.006	0.155	0.161	0.006
15	50.75	0.130	0.168	0.0376	0.113	0.168	**0.055**	0.113	0.168	0.055
16	53.25	0.130	0.173	**0.0428**	0.174	0.174	0.000	0.173	0.173	0.000
17	55.75	0.154	0.178	0.0243	0.123	0.181	0.058	0.120	0.178	**0.058**
18	61.25	0.175	0.190	0.0151	0.191	0.195	0.004	0.185	0.190	0.004
19	69.25	0.185	0.208	0.0232	0.191	0.217	0.027	0.182	0.208	0.027
20	75.75	0.216	0.224	0.0076	0.212	0.235	0.023	0.201	0.224	0.023
21	78.25	0.220	0.230	0.0100	0.225	0.242	0.017	0.213	0.230	0.017
22	80.25	0.186	0.235	0.0488	0.223	0.248	0.025	0.209	0.235	0.025
23	83.75	0.222	0.244	0.0212	0.231	0.258	0.026	0.217	0.244	0.026
24	85.25	0.199	0.247	0.0486	0.253	0.262	0.009	0.238	0.247	0.009
25	87.75	0.231	0.254	0.0225	0.238	0.269	0.031	0.223	0.254	0.031
26	88.75	0.235	0.256	0.0207	0.232	0.272	0.040	0.216	0.256	0.040
27	92.75	0.227	0.266	0.0393	0.243	0.284	0.041	0.226	0.266	0.041
28	95.75	0.268	0.274	0.0063	0.260	0.292	0.032	0.242	0.274	0.032
29	97.25	0.277	0.278	0.0014	0.275	0.297	0.022	0.256	0.278	0.022
30	*99.25*	0.276	*0.283*	0.0074	0.284	*0.303*	0.018	0.265	*0.283*	0.018
MAPE		*2.047%*			*1.855%*			*1.855%*		

been observed for the $I'k$ and *Ip,* respectively. Note that the maximum MAPE is limited to 2.047% as observed at bus 5 for the component I_k''. These results prove the capability of the developed ANN-results of the proposed ANN-based estimation of the SC components at randomly chosen scenarios of PV penetrations. The proposed ANN-based tool have shown

TABLE 3. Validation of the Proposed ANN-based SC Estimation Tool at Bus 8.

No.	p	$I_{k"}$			I_k			Ip		
		SC_p^{Actual}	$SC_p^{Predicted}$	Error	SC_p^{Actual}	$SC_p^{Predicted}$	Error	SC_p^{Actual}	$SC_p^{Predicted}$	Error
1	0.75	0.875	0.875	0.000	0.755	0.756	0.000	0.875	0.875	0.000
2	3.25	0.521	0.522	0.001	0.345	0.345	0.001	0.521	0.522	0.001
3	5.25	0.374	0.377	0.003	0.237	0.238	0.001	0.374	0.377	0.003
5	11.25	0.194	0.211	0.017	0.134	0.139	0.005	0.194	0.211	0.017
6	12.25	0.192	0.198	0.007	0.125	0.133	0.007	0.192	0.198	0.007
7	14.75	0.140	0.176	0.036	0.102	0.123	0.020	0.140	0.176	0.036
8	19.25	0.134	0.153	0.019	0.081	0.116	0.035	0.134	0.153	0.019
9	24.25	0.104	0.143	0.039	0.102	0.116	0.014	0.104	0.143	0.039
10	28.75	0.101	0.141	0.040	0.116	0.121	0.005	0.101	0.141	0.040
11	34.75	0.122	0.144	0.021	0.105	0.132	0.027	0.122	0.144	0.021
12	39.75	0.122	0.150	0.028	0.130	0.142	0.012	0.122	0.150	0.028
13	43.25	0.152	0.155	0.003	0.106	0.150	0.044	0.152	0.155	0.003
14	47.25	0.104	0.161	0.057	0.127	0.159	0.032	0.104	0.161	**0.057**
15	50.75	0.166	0.168	0.002	0.132	0.168	0.036	0.166	0.168	0.002
16	53.25	0.149	0.173	0.024	0.136	0.174	0.038	0.149	0.173	0.024
17	55.75	0.157	0.178	0.021	0.155	0.181	0.026	0.157	0.178	0.021
18	61.25	0.190	0.190	0.000	0.158	0.195	0.037	0.190	0.190	0.000
19	69.25	0.207	0.208	0.001	0.209	0.217	0.008	0.207	0.208	0.001
20	75.75	0.196	0.224	0.028	0.210	0.235	0.025	0.196	0.224	0.028
21	78.25	0.176	0.230	0.053	0.221	0.242	0.022	0.176	0.230	0.053
22	80.25	0.176	0.235	**0.059**	0.235	0.248	0.013	0.176	0.235	0.059
23	83.75	0.209	0.244	0.034	0.229	0.258	0.029	0.209	0.244	0.034
24	85.25	0.231	0.247	0.017	0.212	0.262	**0.050**	0.231	0.247	0.017
25	87.75	0.233	0.254	0.021	0.242	0.269	0.027	0.233	0.254	0.021
26	88.75	0.222	0.256	0.034	0.241	0.272	0.031	0.222	0.256	0.034
27	92.75	0.212	0.266	0.054	0.272	0.284	0.012	0.212	0.266	0.054
28	95.75	0.261	0.274	0.013	0.258	0.292	0.034	0.261	0.274	0.013
29	97.25	0.253	0.278	0.025	0.280	0.297	0.017	0.253	0.278	0.025
30	99.25	0.274	0.283	0.009	0.270	0.303	0.033	0.274	0.283	0.009
MAPE		*2.221%*			*1.129%*			*2.220%*		

marginal errors in predicting the SC current components at bus 8 when compared with those calculated using steady-state simulation based on the IEC 60909 standards. Like the case of Bus 5, the actual values of the current components at Bus 8, (in A), can be obtained by using the estimated values of the ANN-based estimation tool that have been multiplied by the original maximum values as follows: $I_k'' = 5743.29$ A, $I_k' = 4637.27$A, and $Ip = 8122.23$ A.Observe Table 3 which shows that a maximum absolute error of 0.059 has been registered for $I =_{k,}$ at the scenario of 22% penetration. While lower error values of 0.050 and 0.057 have been observed for the I_k' and Ip, respectively. On the other hand, the maximum MAPE is limited to 2.221% as observed at bus 8 for the component I_k''. It is worth mentioning that the effect of the Bus location on the accuracy of the proposed ANN-based estimation tool is marginal. It can be observed from Tables 2 and 3 that Bus 8 which has a higher original fault level (i.e. located closer to the generation centers), shows a lower accuracy when it comes to estimating both the sub-transient SC current, I_k'', and the peak SC current, Ip, but shows a higher accuracy when estimating the and the transient SC current, I_k'. Taken together, all the above illustrated figures illustrate the efficacy of the proposed ANN-based estimation tool at the variety of scenarios and locations when applied to newly randomly chosen penetration scenarios with an average of MAPE of 1.89%. In other words, the average accuracy of the proposed ANN-based SC estimation tool is 98.11% approximately.

VI. CONCLUSION

In this paper, an ANN-based tool has been developed and validated for the estimation/forecasting of the SC currents in power systems rich of PE-based RESs, mainly PV systems. The proposed ANN-based tool relies on the online penetration level of the PE-based RESs as an input fed to the ANN for estimating the SC current components accordingly. The development stage involves the training of the proposed SC estimation tool with the SC currents collected for large number of scenarios that have been simulated offline on the modified IEEE-9 bus test system modelled in DIgSILENT PowerFactory software. The fault calculations have been done by steady-state simulations based on the IEC 60909 standards. The training phase of the developed ANN includes anticipating of the best structure and the best training performance that have been identified using the values of the statistical indicator (MSE) and the Regression (R). Thus, a Feedforward back propagation ANN structured of one input layer with one input (the penetration percentage of PV, p), one hidden layer of 20 neurons, and an output layer of 6 outputs has been picked as it has provided the best performance. Note that 200 samples of outputs associated with each of the current component, that represents 200 scenarios of PV penetration, are chosen for training, validation, and testing of the results obtained at each bus. These estimated outputs are: the subtransient SC current, I_k'', the transient SC current, $I_{k'}$, and the peak SC current, I_p, three for the studied bus 5 and three for the bus 8. It worth mentioning that the values of the collected SC currents have shown new mixed characteristics that is different from what has been traditionally observed in traditional power systems with SGs only.

All the components of the total SC current show maximum values at the base scenario ($p = 0\%$), before showing decaying behaviour when reaching the minimum values at around the to their minimum at around the scenario of ($p = 30\%$). Then, they experience a steady increase to a higher level at the last scenario of ($p = 100\%$). This implies that the dominated SC contribution before reaching ($p = 30\%$) scenario, while the SC contribution of the PE-based RESs will be the dominated elsewhere after that till reaching the scenario of (p=100%).

The generalization capability of the proposed ANN-based SC current estimation tool is also examined using new input/output testing pattern sets of different percentages of PE-based RESs penetrations obtained from untrained scenarios. The accuracy of the proposed ANN-based tool is validated by comparing the actual and the estimated results represented by the absolute error of each component of the SC current at each scenario. In addition, the overall accuracy has also been evaluated using the mean absolute percentage error (MAPE) considering all the simulated scenarios simultaneously. The results have proven the applicability of the proposed ANN-based tool in estimating the SC current components at various range of PE-based RESs penetration scenarios, with an overall accuracy of 98.11%.

Taken together, it can be concluded that, when employed, the developed ANN-based tool can provide a powerful technique for fast and effective estimation of the SC currents in future power systems with high penetration of PE-based RESs systems at different locations by one input only, namely, the penetration percentage of PE-based RESs in the system. In other words, these results show the effectiveness of the developed tool in mapping the SC current with the penetration percentage of PE-based RESs, hence, providing accurate insight on the estimated SC currents and the expected fault current shortfalls that may be experienced in future RESs-rich power systems with the knowledge of the penetration level scenario without a need for detailed modeling or repetitive calculations at each newly faced scenario. Although this proposed ANN-based has been applied to estimate SC currents at some selected buses/nodes in this work, it can also be applied, when required, to estimate the SC currents at different areas, subsystems, and nodes depending on the availability of the training dataset. It is worth noting that this proposed ANN-based SC estimation tool is limited in this work to the PE-based RESs that utilize full-size converters such as (PV and type-4 wind generators). Also, it is pointing out that changing the system topology or the PV penetration scenarios like introducing PVs to non-generation buses might require a new structured ANN and larger dataset for training depending on the topology and the size of the network. These provide a headroom for potential improvements by including other types of RESs such as DFIG wind generators, application of the methodology to other systems with different topologies and a wider range of RESs penetration scenarios, and practical implementation of a test case using real-time data as future work.

REFERENCES

[1] B. S. Hodge, H. Jain, C. Brancucci, G. Seo, M. Korpas, J. Kiviluoma, H. Holttinen, J. C. Smith, A. Orths, A. Estanqueiro, L. Söder, D. Flynn, T. K. Vrana, R. W. Kenyon, and B. Kroposki, "Addressing technical challenges in 100% variable inverter-based renewable energy power systems," *WIREs Energy Environ.*, vol. 9, no. 5, p. e376, Sep. 2020.

[2] F. Milano, F. Dorfler, G. Hug, D. J. Hill, and G. Verbic, "Foundations and challenges of low-inertia systems (invited paper)," in *Proc. Power Syst. Comput. Conf. (PSCC)*, Jun. 2018, pp. 1–25.

[3] S. Impram, S. V. Nese, and B. Oral, "Challenges of renewable energy penetration on power system flexibility: A survey," *Energy Strategy Rev.*, vol. 31, Sep. 2020, Art. no. 100539.

[4] R. R. Aljarrah, "Assessment of fault level in power systems with high penetration of non-synchronous generation," Ph.D. dissertation, School Elect. Electron. Eng., Univ. Manchester, UoM. U.K., 2020.

[5] J. Keller and B. Kroposki, "Understanding fault characteristics of inverter-based distributed energy resources," Nat. Renew. Energy Lab., NREL, Golden, CO, USA, Tech. Rep., NREL/TP-550-46698, 2010.

[6] C. A. Plet, M. Graovac, T. C. Green, and R. Iravani, "Fault response of grid-connected inverter dominated networks," in *Proc. IEEE PES Gen. Meeting*, Jul. 2010, pp. 1–8.

[7] R. J. Nelson, "Short-circuit contributions of full converter wind turbines," in *Proc. Transmiss. Distribution Conf. Expo.*, May 2012, pp. 1–5.

[8] T. Neumann and I. Erlich, "Short circuit current contribution of a photovoltaic power plant," *IFAC Proc. Volumes*, vol. 45, no. 21, pp. 343–348, 2012.

[9] J. C. Quispe H, H. Villarroel-Gutierrez, and E. Orduna, "Analyzing short-circuit current behavior caused by inverter-interfaced renewable energy sources. Effects on distance protection," in *Proc. IEEE PES Transmiss. Distrib. Conf. Exhib.*, Sep. 2020, pp. 1–6.

[10] S. Liu, T. Bi, and Y. Liu, "Theoretical analysis on the short-circuit current of inverter-interfaced renewable energy generators with fault-ride-through capability," *Sustainability*, vol. 10, no. 2, p. 44, Dec. 2017.
[11] J. Fortmann, R. Pfeiffer, E. Haesen, F. Hulle, F. Martin, H. Urdal, and S. Wachtel, "Fault-ride-through requirements for wind power plants in the ENTSO-E network code on requirements for generators," *IET Renew. Power Gener.*, vol. 9, no. 1, pp. 18–24, Jan. 2015.
[12] M. T. Hagh and T. Khalili, "A review of fault ride through of PV and wind renewable energies in grid codes," *Int. J. Energy Res.*, vol. 43, no. 4, pp. 1342–1356, Mar. 2019.
[13] S. Yuan, B.-F. Yang, and J.-Y. Zhang, "Experimental study on short-circuit current characteristics of a photovoltaic system with low voltage ride through capability under a symmetrical fault," *Energy Rep.*, vol. 8, pp. 4502–4511, Nov. 2022.
[14] C. A. Plet and T. C. Green, "Fault response of inverter interfaced distributed generators in grid-connected applications," *Electric Power Syst. Res.*, vol. 106, pp. 21–28, Jan. 2014.
[15] N. Baeckeland, B. Herteleer, and M. Kleemann, "Modelling fault behaviour of power electronic converters," *Int. J. Electr. Power Energy Syst.*, vol. 123, Dec. 2020, Art. no. 106230.
[16] C. Plet, M. Brucoli, J. D. McDonald, and T. C. Green, "Fault models of inverter-interfaced distributed generators: Experimental verification and application to fault analysis," in *Proc. IEEE Power Energy Soc. Gen. Meeting*, Jul. 2011, pp. 1–8.
[17] L. Wang, H. Gao, and G. Zou, "Modeling methodology and fault simulation of distribution networks integrated with inverter-based DG," *Protection Control Modern Power Syst.*, vol. 2, no. 1, pp. 1–9, Dec. 2017.
[18] N. Zhou, J. Wu, and Q. Wang, "Three-phase short-circuit current calculation of power systems with high penetration of VSC-based renewable energy," *Energies*, vol. 11, no. 3, p. 537, Mar. 2018.
[19] R. Aljarrah, H. Marzooghi, J. Yu, and V. Terzija, "Monitoring of fault level in future grid scenarios with high penetration of power electronics-based renewable generation," *IET Gener., Transmiss. Distrib.*, vol. 15, no. 2, pp. 294–305, Jan. 2021.
[20] H. Liu, K. Xu, Z. Zhang, W. Liu, and J. Ao, "Research on theoretical calculation methods of photovoltaic power short-circuit current and influencing factors of its fault characteristics," *Energies*, vol. 12, no. 2, p. 316, Jan. 2019.
[21] R. Aljarrah, H. Marzooghi, J. Yu, and V. Terzija, "Sensitivity analysis of transient short circuit current response to the penetration level of non-synchronous generation," *Int. J. Electr. Power Energy Syst.*, vol. 125, Feb. 2021, Art. no. 106556.
[22] *Short-Circuit Currents in Three-Phase AC Systems, Part 0: Calculation of Currents*, IEEE Standard 60909, 2016.
[23] G. Balzer, "Short-circuit calculation with fullsize converters according to IEC 60909," in *Proc. 21st Conf. Electric Power Supply Ind.*, 2016, pp. 1–9.
[24] R. Aljarrah, H. Marzooghi, V. Terzija, and J. Yu, "Modifying IEC 60909 standard to consider fault contribution from renewable energy resources utilizing fully-rated converters," in *Proc. 9th Int. Conf. Power Energy Syst. (ICPES)*, Dec. 2019, pp. 1–6.
[25] E. S. N. R. Paidi, H. Marzooghi, J. Yu, and V. Terzija, "Development and validation of artificial neural network-based tools for forecasting of power system inertia with wind farms penetration," *IEEE Syst. J.*, vol. 14, no. 4, pp. 4978–4989, Dec. 2020.
[26] O. I. Abiodun, A. Jantan, A. E. Omolara, K. V. Dada, N. A. Mohamed, and H. Arshad, "State-of-the-art in artificial neural network applications: A survey," *Heliyon*, vol. 4, no. 11, Nov. 2018, Art. no. e00938.
[27] D. Solyali, "A comparative analysis of machine learning approaches for short-/long-term electricity load forecasting in Cyprus," *Sustainability*, vol. 12, no. 9, p. 3612, Apr. 2020.
[28] S. Wang, "Artificial neural network," in *Interdisciplinary Computing in Java Programming*. Berlin, Germany: Springer, 2003, pp. 81–100.
[29] E. Feilat, R. Aljarrah, and M. Rifai, "Detection and classification of voltage variations using combined envelope-neural network based approach," *Jordan J. Electr. Eng.*, vol. 3, no. 2, p. 113, 2017.
[30] K. Sheela and S. Deepa, "Review on methods to fix number of hidden neurons in neural networks," *Math. Problems Eng.*, vol. 2013, pp. 1–11, May 2013.
[31] V. Vittal, J. McCalley, P. Anderson, and A. Fouad, *Power System Control and Stability*. Hoboken, NJ, USA: Wiley, 2019.